Scaling Characteristics of Ground Vortices in a Nacelle Inlet Flow Field

Derek A. Nichols[1], Bojan Vukasinovic[2], and Ari Glezer[3]
Georgia Institute of Technology, Atlanta, GA 30332-0405

Abstract

The formation of a ground vortex in the suction flow field of an axisymmetric nacelle inlet in close proximity to a ground plane and in the presence of crosswind normal to the nacelle's axis is investigated in low-speed wind tunnel experiments. It is shown that the vortex formation over the ground plane is effected by interactions between the nacelle's near wake and near-surface, countercurrent shear that is induced between the crosswind and opposing direction inlet suction flow. The ensuing vortex is precipitated by progressive deflection of the wake towards the ground plane downstream of the inlet. For a given elevation ratio of the nacelle relative to the ground plane, the formation of the ground vortex is governed by the critical intake thrust coefficient (ratio of nacelle thrust to crosswind momentum through the inlet area). The vortex forms above the critical thrust coefficient, is ingested along the inlet's lower leeward side, and is advected towards the windward side as the thrust coefficient increases. It is also shown that the critical thrust coefficient required to form a ground vortex increases quadratically with the nacelle elevation and that, at a given ground plane distance and thrust coefficient, the inlet flow field scales with the crosswind speed.

Nomenclature

D	=	inlet throat diameter
H	=	height of inlet centerline from ground
h	=	ground plane distance from inlet base
$\dot{m}$	=	inlet mass flow rate
$\dot{m}_c$	=	inlet mass flow rate at choking
$\dot{m}^*$	=	$\dot{m}/\dot{m}_c$
p_a	=	atmospheric pressure
p_o	=	total pressure
r'	=	distance from inner inlet wall
R	=	inlet throat radius
T	=	thrust
T^*	=	thrust coefficient
T^*_{crit}	=	thrust coefficient required to form vortex
$\bar{u}$	=	mean velocity component along wind tunnel
U_o	=	crosswind speed
V	=	average inlet velocity
V'	=	inlet velocity at the shear layer interface
$\bar{w}$	=	mean vertical velocity component
x	=	horizontal displacement from inlet centerline
y	=	streamwise displacement from inlet face
z	=	vertical displacement from inlet centerline
θ	=	azimuthal coordinate
ρ	=	ambient air density

[1] Graduate Research Assistant, AIAA Member.
[2] Senior Research Engineer, AIAA Member.
[3] Professor, AIAA Fellow.

I. Background

Commercial aircraft engine nacelles must be designed to comply with the Code of Federal Regulations (CFRs) throughout all stages of flight (including ground taxi, takeoff, climb, cruise, descent, and landing). Even though most of the flight time is spent in cruise, the optimal design of the nacelle for cruise conditions must be adjusted to accommodate for operation at lower speed for takeoff and landing and close to the ground where the performance of the aircraft engines can be strongly impacted by the presence of the ground surface and crosswind that can significantly alter the air intake at the inlet [1]. Specifically at low aircraft speed, a crosswind can lead to the formation of a fuselage vortex, induce inlet flow separation, and, near the ground, create a ground vortex [2,3].

Inlet flow separation can occur as a result of crosswind or during climb at steep angles [4,5]. Earlier experimental investigations at Georgia Tech focused on the characterization of this separation for a range of intake and crosswind speeds [6,7], and the utility of several of passive and active flow control methodologies for mitigation and suppression of ensuing internal separation on the windward side [6–8].

In addition to inlet flow separation, when in close proximity to the ground plane, the crosswind can also lead to the formation of a ground vortex that induces distortion within the inlet plane and can also lead to the ingestion of foreign objects into the engine. As discussed by Colehour and Farquhar [2] at that time (1971) about 50% of all engines removed from aircraft had been damaged by ingestion of foreign objects. Such ingestion by a ground vortex was first investigated by Klein [9], and its formation with varying engine height, engine speed, and crosswind speed (referred to here as the vortex 'formation parameters') was initially proposed by Rodert and Garret [10] who suggested that the formation of the ground vortex required a stagnation point on the ground plane. This stagnation point is the result of the inlet's capture surface reaching and subsequently interacting with the ground plane [11]. Johns [12] discusses how this capture surface can change in the presence of a crosswind, headwind, or tailwind. The work of Liu et al. [13] was the first to demonstrate a linear relationship between the velocity ratio of the mean intake and crosswind speeds V/U_o for which a ground vortex first forms and the elevation of the inlet above ground which is expressed by the ratio of the inlet's height to its diameter. Shin et al. [14] compared Liu et al.'s data with inlets of varying size and orientation and reported similar results, and Nakayama and Jones improved further on this fit by including data for cases involving small H/D and high Mach numbers [15,16].

Once the ground vortex forms, its flow characteristics change with the three formation parameters. Perhaps the first analysis of these changes was reported by Shin et al. [14] who measured the ground vortex circulation in wind tunnel experiments while changing the velocity ratio, V/U_o, and the ground plane distance ratio, H/D. It was observed that the vortex strength as measured by its circulation increases with the velocity ratio and decreases with the ground plane distance. Brix et al. [17] performed more comprehensive wind tunnel experiments and noted that the circulation of the vortex increases by increasing the circulation around the inlet with increased U_o or increasing the circulation by vortex stretching with V. Siervi [11, 18] placed two inlets on top of one another in the absence of a ground plane and observed that a vortex still formed between them, concluding that the surface boundary layer was not the primary source of vorticity leading to the vortex generation. However, in more recent numerical investigations, Trapp and Girardi [3] found that the formation of the vortex depends on the presence of a source of vorticity in the flow field and showed that the vortex characteristics depend on vorticity that is generated on the ground plane

American Institute of Aeronautics and Astronautics

[3]. These differences in the attributes to the source of vorticity were explained by Siervi [11] who suggested two competing mechanisms for the inlet vortex formation associated with ground boundary layer vorticity and variation of circulation along the nacelle by the crosswind.

Murphy et al. [19] studied the effect of a horizontally moving ground plane to simulate realistic takeoff conditions at low velocity ratios between the crosswind and intake speeds and noted that, compared to a stationary ground plane, a ground vortex on a moving ground plane was weaker, steadier, and more symmetric relative to the static ground. Murphy and MacManus [20] considered the effects of the ground plane height and the yaw angle of the crosswind and showed that a stronger vortex formed at lower ground plane clearances and higher intake yaw angles. Several simulations demonstrated suppression of the ground vortex using external jets such as fan reverser jets [12,21], pulsed jets [12,21], and sprinkler jets [22]. Notably, the simulations of Shmilovich and Yadlin [22] showed that ground vortex ingestion can be completely suppressed by using 'sprinkler' jet actuation.

The present experimental investigation is a continuation of the earlier work of Nichols et al. [23] that focused on the characterization of the ground vortex in terms of its circulation and position relative to the nacelle. The present work focuses on the causality between the inlet flow field and ground vortex formation for a broad range of formation parameters with specific attention to the underlying mechanisms of changes in the flow field that precipitate the onset of vortex formation. The ensuing flow fields for different formation parameters are scaled to demonstrate similarity in terms of the thrust coefficient and ground plane elevation.

II. Experimental Setup and Flow Diagnostics

The present experimental investigation is conducted in an open-return wind tunnel which was specifically designed to investigate the flow physics of nacelles in crosswind. The wind tunnel's test section has an adjustable ground plane and includes a model nacelle assembly mounted through its side wall, as shown Figure 1. The axisymmetric nacelle model (throat inlet diameter D) with conical centerbody of diameter $0.3D$ is mounted onto an axisymmetric duct that is driven in suction by a computer-controlled blower whose exhaust is released into the ambient air through chilled water heat exchangers such that the ambient air temperature is maintained to within 1°C. The nacelle blower assembly is mounted on a moveable cart that enables its axial and lateral position within the test section to be adjusted. In the present investigation, the nacelle model is oriented normal to the cross flow and extends through half the width of the test section. The blower is driven at a prescribed mass flow rate $\dot{m}$ that is monitored using a pitot probe assembly within a calibrated straight pipe segment upstream of the blower's inlet (the nacelle duct chokes at some critical $\dot{m}_c$ which is used to define the present mass flow parameter $\dot{m}^* = \dot{m}/\dot{m}_c$). As noted above, the tunnel's test section is equipped with a vertically-adjustable ground plane (to within 0.25 mm) that can be lowered up to $h = 1.6D$ below the bottom edge of the nacelle (Figure 2a). The cross flow in the test section is generated by an open-return, low-speed wind tunnel with a contraction ratio of 10:1 that is driven by a computer-
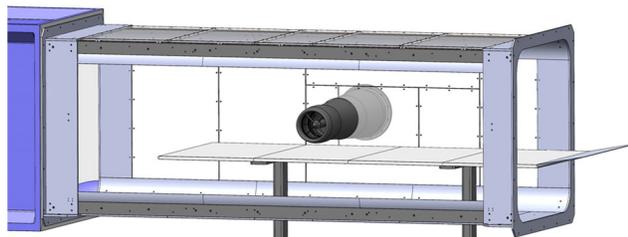

Figure 1. *The crosswind wind tunnel test section showing the installed axisymmetric inlet and the vertically-adjustable ground plane.*

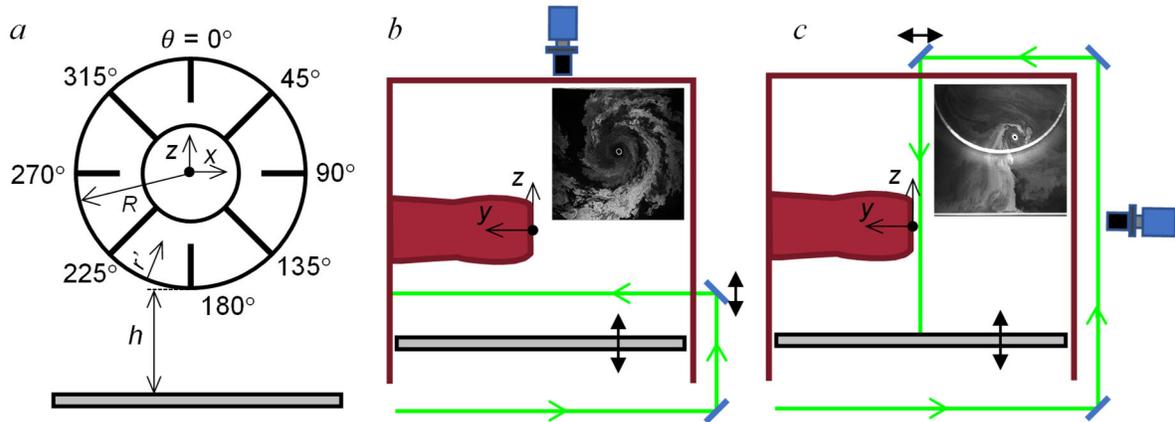American Institute of Aeronautics and Astronautics

Figure 2. *A rake of the total pressure probes relative to the ground plane (a) and the schematics of the PIV setup with horizontal (b) and vertical (c) flow illumination. Inset images illustrate the corresponding fields of view.*

controlled axial blower (flow uniformity in the empty test section within 1%). The present investigations emulate crosswind speeds up to $U_o = 35$ knots (18.0 m/s).

Pressure recovery and flow distortion within the nacelle are assessed using a total pressure rake assembly that is located $0.43D$ downstream of the nacelle's lip at the characteristic position of the fan face. The assembly consists of 8 radial rakes that are equally distributed azimuthally (45°) with $\theta = 0°$ at the top of the inlet and increasing clockwise while alternating between 8 and 10 total pressure probes each, as shown in Figure 2a, with a higher density of probes closer to the wall. The rake total pressures are measured with a dedicated 96-channel pressure scanner with an uncertainty better than 1% of the time-averaged sample. The flow is also characterized using planar particle image velocimetry (PIV) as illustrated in Figures 2b-c where the laser sheet is oriented either parallel to the ground plane (Figure 2b) or parallel to the inlet face (Figure 2c) to allow for tracking the motion of the ground vortex and extracting its velocity field. Inset images illustrate instantaneous seeded flow for both configurations. The horizontal laser sheet illumination (Figure 2b) targets the vortex formation and near-ground motion, while the vertical laser sheet view (Figure 2c) enables vortex tracking at the inlet face, as well as the characterization of the nacelle's external flow field.

In the present investigations, the vortex formation parameters including the nacelle's mass flow rate, crosswind speed, and ground plane distance are each independently controlled, and all characterizations are done past the transients associated with any parameter variation, i.e., all the results concern the quasi-steady/steady flow states

III. The Ground Vortex Effect on the Inlet Flow Field

As it has been known for decades (cf. Section I), when in the proximity of a horizontal ground plane, the flow through an inlet in a cross flow is susceptible to the formation of a ground vortex. An example of the realization of such a vortex in the present experiments is shown in Figure 3, where the flow in the test section is seeded with theatrical fog (the crosswind flow moving from left to right), and the nacelle's inlet plane is illuminated with a spanwise-normal laser sheet as shown in Figure 2c, where the bright horizontal line at the bottom of Figure 3 shows the laser sheet reflecting off the ground plane. The typical vortex of the clockwise (CW) sense of vorticity is seen

rising off the ground plane and is subsequently ingested along the nacelle's inner lower lip. Even though the seeding particles do not reach the center of the vortex core, the core is accentuated by a bright ring of condensed water vapor resulting from the low pressure associated with the vortex core which in this case is lower than the ambient dew point pressure.
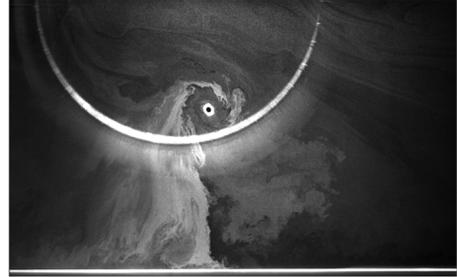
The conditions which produce the onset of the formation of an ingested ground vortex have been studied extensively in previous work [23]. As discussed, just before the onset of an ingested ground vortex, vortices

Figure 3. *A sample image of the fog-seeded ground vortex with cross flow moving from left to right.*

begin to occasionally develop in the shear layer between the opposing direction crosswind and intake flow on the leeward side of the inlet. Such a countercurrent shear layer is demonstrated in Figure 4 where a PIV color raster plot of the time-averaged streamwise velocity distribution superposed with uniform length velocity vectors is plotted within a horizontal plane measuring $0.7D \times 0.7D$ which is $0.14D$ above the ground plane and on the outer edge of the inlet, as illustrated in the bottom row. The flow conditions are selected to be just before the onset of a stable/ingested vortex for which $\dot{m}^* = 0.65$, $U_o = 30$ kt, and $h/D = 0.36$. The lower half of this field shows the crosswind moving nearly uninhibited across the domain; however, at the top left of the field, the flow moves in the opposite streamwise direction presumably due to the suction effect of the inlet.
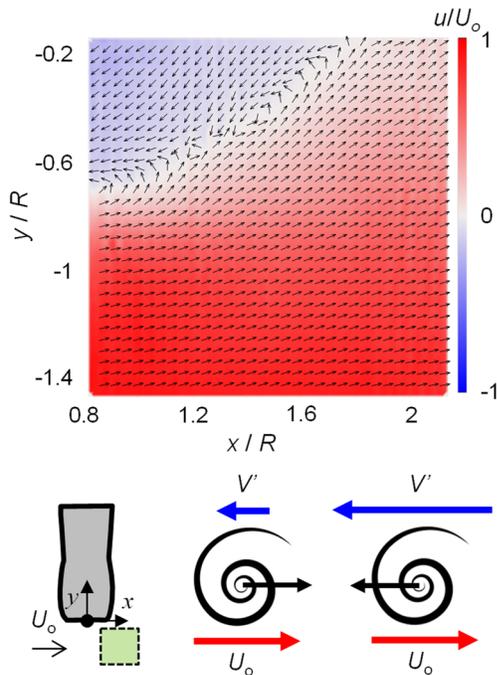

Figure 4. *Time-averaged PIV color raster plot of the streamwise velocity component superposed with equal length velocity vectors at z/R = -1.43 (the measurement plane is shown relative to the nacelle in the inset). The data are taken for h/D = 0.36, $\dot{m}^*$ = 0.65, and U_o = 30 kt.*

In between these two flows, a crescent-shaped boundary is formed, along which the streamwise velocity vanishes, in the average sense. It is observed that vortices originate within this countercurrent shear layer, apparently as the result of a Kelvin-Helmholtz instability, and initially move in the direction of the prevailing velocity in this shear layer. If the crosswind speed is higher at this interface, then the vortex will shed downstream with the crosswind. If the intake speed is higher at this interface, however, then the vortex will instead move upstream and become ingested into the inlet. This vortex that is formed initially is highly unstable due to the switching in the prevailing local flow direction and is located fairly high on the leeward side ($\theta = 135°$) which is characteristic of vortices which have just formed or are about to dissipate [23]. As the inlet suction further intensifies, the intake flow in this shear layer prevails at all times and the vortex stabilizes as it is ingested into the inlet. If say, the ground plane distance begins to increase while the stable vortex is already formed, the streamwise countercurrent inlet flow weakens and the ingested vortex migrates towards the leeward inner lip until it eventually is pulled outside of the inlet and 'dissipates' in the downstream crosswind direction.
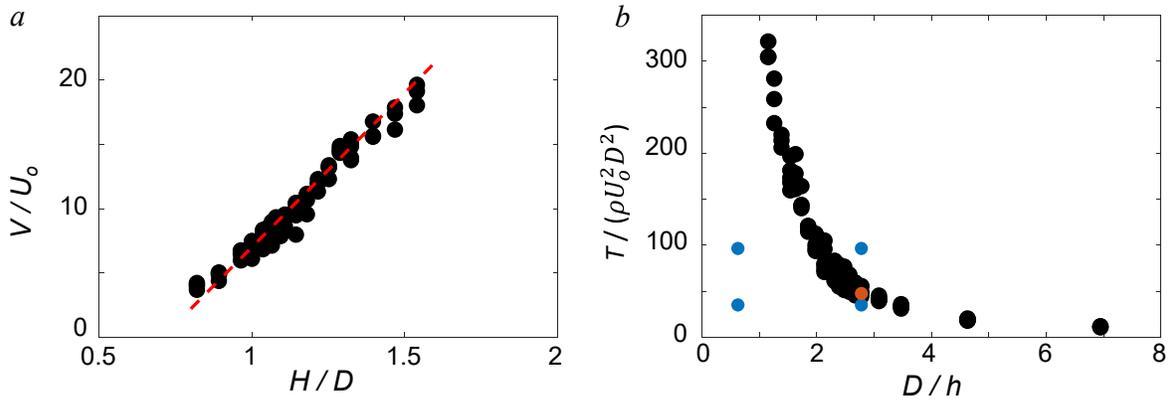
Figure 5. *Conditions for which a vortex first forms (●) for ratio of average intake and crosswind speed (a), and for the ratio of thrust and crosswind momentum (b). Fit from Nakayama and Jones [15] shown in (a) for reference. Additional points (●, ●) in (b) refer to Figures 4 and 6.*

The critical conditions necessary for a ground vortex to form have been established by Liu et al. [13] and Shin et al. [14] and are expressed by Nakayama and Jones [15] in terms of the velocity ratio between the intake speed and crosswind speed assuming that the density of the flows remains unchanged (Equation 1) where V is the average velocity of the inlet and H is the height of the inlet centerline from the ground plane. Any conditions above this line will form a ground vortex whereas anything below will not. The critical conditions for vortex formation were also previously measured for a range of intake speeds, crosswind speeds, and ground plane distances by Nichols et al. [23] and are replotted in Figure 5a in terms of V/U_o = f (H/D), where Eq. (1) is also shown as a dashed line for reference. Clearly, a very good agreement of the present results and these prior findings can be seen in this plot.

$$\frac{V}{U_o} = 24\frac{H}{D} - 17 \qquad (1)$$

$$T_{crit}^* = \left(\frac{T}{\rho U_o^2 D^2}\right)_{crit} = 375\left(\frac{h}{D}\right)^2 \qquad (2)$$

However, it can be argued that the scaling proposed by Nichols et al. [23] may bear a deeper physical meaning of the flow conditions critical for the ground vortex formation. Hence, the thrust through the inlet is scaled by the equivalent crosswind momentum through the inlet projected area, as shown in Figure 5b. Such a proposed relationship separates realizable vortical states (above) from the flow states without ground vortices (below). On one side, as the ground plane distance increases, the inlet/engine thrust must also increase sharply to enable the ground vortex formation, clearly indicating that the ground vortex state would be eventually unattainable as the inlet/plane distance from the surface increases. Conversely, as the ground plane distance deceases, the critical inlet thrust for the vortex formation decreases, asymptotically approaching a small but nonzero thrust such that it is possible for a ground vortex to form even at a very low engine thrust. This alternative relationship is shown in Eq. (2) in its functional form, relating the critical thrust with the dimensionless ground plane distance from the inlet of diameter D. For reference, the flow condition discussed in Figure 4, representing the onset of vortex initiation, is marked by an orange circle in Figure 5b.
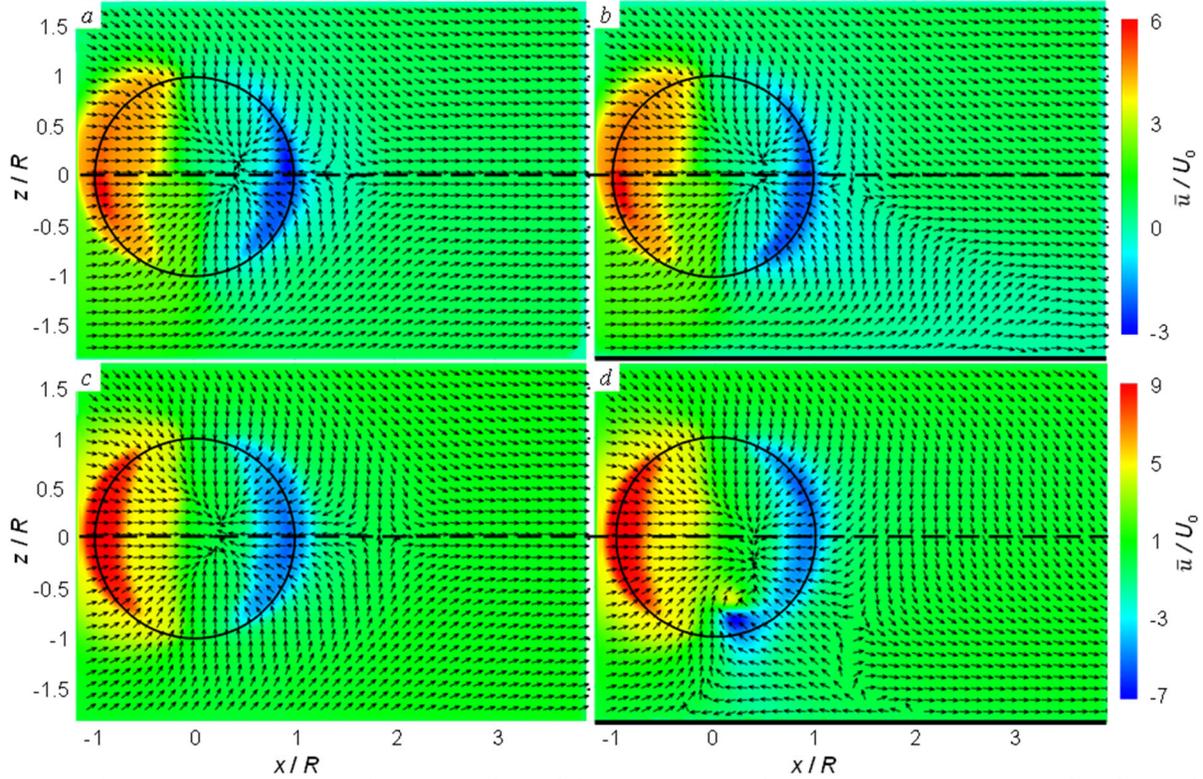
American Institute of Aeronautics and Astronautics

Figure 6. *Time-averaged PIV color raster plots of the streamwise velocity component superposed with equal-length velocity vectors at the inlet face for $\dot{m}^* = 0.2$ (a-b) and 0.3 (c-d) and ground plane distances of $h/D = 1.60$ (a,c) and 0.36 (b,d). The inlet contour, inlet horizontal centerline, and ground plane are superposed for reference.*

The onset of the ground vortex leads to significant changes in the overall flow field about the nacelle inlet. To demonstrate these changes, the two inlet mass flow rates of $\dot{m}^* = 0.2$ and 0.3 and the two ground plane distances of $h/D = 1.60$ and 0.36 are considered, selected such that, for the closest ground plane distance, one mass flow rate results in the ground vortex formation while the other does not – these four flow states are also marked in Figure 5b by blue circles. For each of these conditions, a PIV color raster plot of the time-averaged streamwise velocity is plotted superposed with fixed-length velocity vectors within a vertical plane located just upstream of the inlet face. A contour of the inlet lip is included for reference. As seen in each of the flow fields, the streamwise component of the outer flow reaches that of the cross-stream speed, i.e., $\bar{u} \approx U_o$, while the streamwise component in the inlet vicinity is greatly affected by the inlet intake flow. Consider first the case of the lower intake mass flow rate $\dot{m}^* = 0.2$ (Figures 6a-b). When the ground plane is sufficiently displaced, where $h/D = 1.60$ (Figure 6a), the flow is reasonably symmetric about the horizontal axis. A notable characteristic of this flow field is an apparent sink within the inlet which represents the point of zero in-plane velocity implying only out-of-plane motion. Another important flow feature is a saddle point on the outer leeward side of the inlet which separates the flow going into the inlet and that forming the wake behind the nacelle. This saddle point is located on the horizontal central plane of the inlet, further indicating the flow symmetry about this plane. When the ground plane distance is decreased to $h/D = 0.36$ (Figure 6b), there are some noteworthy changes in the flow structure. First, the saddle point on the outer leeward side shifts downward slightly and is no longer centered. In tandem with this shift, the entire structure of the wake shifts downward leveling off at approximately $z/R = -1$. This shift is associated with the outward extension of the flow drawn into the inlet down to the ground plane. Therefore, as the

inlet pulls air from the surroundings, some of this air becomes drawn along the ground plane which introduces losses, dropping the velocity of the flow. It is noted that, despite the intake flow interaction with the ground plane, this interaction is not sufficient to induce a ground vortex under these conditions. The ground vortex is not formed for the far ground plane distance even when the mass flow rate of the inlet is increased to $\dot{m}^* = 0.3$ (Figure 6c); the most notable difference is that the saddle point behind the inlet moves further downstream as the outer flow drawn into the inlet expands outward. Another change relative to the lower mass flow rate case is that the location of the sink within the inlet moves towards the windward side, becoming more centralized within the inlet (the sink evolution is explored in greater detail in Figure 7). When the ground plane is moved closer to the inlet for this higher mass flow rate (Figure 6d), there are significant changes in the structure of the flow field. Interaction between the flow drawn into the inlet and the ground plane becomes sufficient to give a rise to a ground vortex. The flow rises off the plane at about $x/R = 0$ which is associated with the vortex and displays characteristic reversed flow at the wall downstream of this point, while the vortex signature at the inlet face in terms of the streamwise velocity magnitude is seen by the strong localized negative velocity domain about $z/R = -1$ around the lower lip. Another significant change in the flow is related to further closing of the wake, where the saddle point shifts well below the horizontal central plane of the inlet, sinking nearly to the inlet base elevation. The vortex ingestion also strongly couples to the inlet sink region which elongates while migrating downward and toward the leeward side.

As seen above, the prevailing sink domain over the inlet face changes with different inlet flow scenarios and can be considered as an indicator of the windward-leeward and top-bottom intake flow symmetry. To further illustrate this point, the case of $\dot{m}^* = 0.3$ and $h/D = 0.36$ is examined at various crosswind speeds ranging from $U_o = 5 - 30$kt. Consequently, the migration of the sink center with increasing crosswind speed is plotted over the leeward bottom quadrant of the inlet in Figure 7. As a reference, the lower leeward quarter of the inlet contour is also shown. At the lowest crosswind speeds 5kt $< U_o < 10$kt, a ground vortex exists within the inlet, and the sink, marked in blue, has a downward offset from the center plane, where this offset grows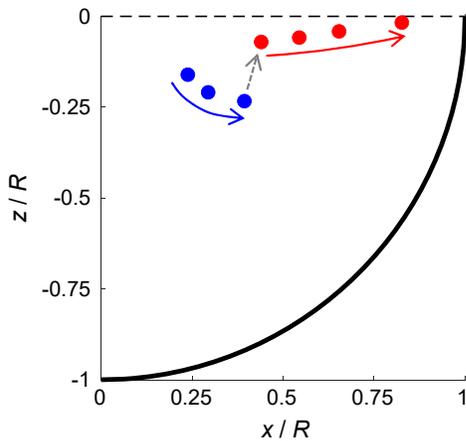 as the crosswind speed increases. Once the crosswind speed increases from $U_o = 10$kt to 15kt, there is a steep jump in the vertical position of the sink, resulting from the disappearance of the ground vortex. Although the vertical intake symmetry becomes greatly restored once the vortex dissipates, some residual asymmetry is still present due to the proximity of the ground plane. This sink center offset (marked in red) decreases as the crosswind speed increases indicating that the vertical symmetry of the flow field nearly returns for the highest crosswind speed, suggesting that the wake flow interaction with the ground plane also relaxes back to insignificant levels. After this crosswind speed exceeds some critical value (for this case $U_o > 30$kt), there is no clear sink within the inlet as all flow measured at the face retains some velocity component parallel to the inlet face due to the relative momentum of the oncoming crosswind flow.

Figure 7. *Evolution of the center of the sink flow at the inlet face for increasing crosswind speeds from left to right, in the presence (●) and absence (●) of a ground vortex. The inlet contour is shown in black for reference.*

Another analysis of the intake flow through the inlet face is done through the mean velocity distributions along the horizontal inlet axis, as shown in Figure 8. Before the vortex forms at $\dot{m}^* = 0.2$ (red), the two streamwise velocity profiles for $h/D = 1.60$ (dashed) and 0.36 (solid) are nearly identical (Figure 8a). The maximum velocity is measured at the windward lip of the inlet ($x/R = -1$), and this velocity linearly decreases across the inlet face and reaches its minimum value at the leeward lip of the inlet ($x/R = 1$). The crossing at zero velocity corresponds to the sink flow intersection, as already discussed in conjunction with Figure 7. It is interesting to note that the difference in the absolute value of the peaks for the streamwise velocity maximum/minimum is approximately 4 as this is a trend that is repeated for additional cases. Downstream of the inlet, the velocity plateaus to $\bar{u}/U_o = 1$ (i.e., at the freestream crosswind speed). Increasing the inlet speed to $\dot{m}^* = 0.3$ (blue), the major difference seen in the streamwise velocity profiles is in the increase in the peak magnitudes; still, the difference of these peak magnitudes remains approximately 4. As the peaks widen, the linear section
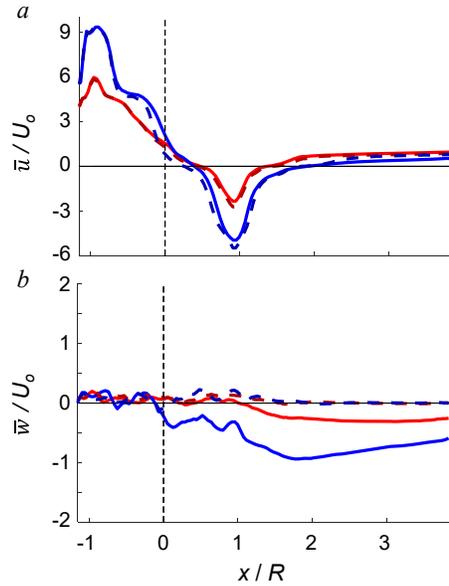

Figure 8. *The mean horizontal (a) and vertical (b) velocities along the horizontal inlet centerline elevation for $\dot{m}^* = 0.2$ (red) and 0.3 (blue) for $h/D = 1.60$ (- -) and 0.36 (-). The inlet's vertical centerline is shown in black dashed for reference.*

of the velocity profile shrinks and becomes confined to the inlet center. It is interesting that no significant difference in the streamwise profiles within the inlet is seen across this horizontal axis between the no-vortex (dashed) and the vortex (solid) states, presumably due to sufficient distance away from the vortex core; however, a minor difference is observed at the farthest distance from the inlet ($x/R > 2$). While the velocity still plateaus to the crosswind velocity for the farther ground plane distance (albeit in a longer timeframe than at the lower intake speed), in the case of the closer ground plane distance (and the formed ground vortex), the streamwise velocity has yet to relax back towards the crosswind speed even at the farthest downstream distances. Distributions of the corresponding mean vertical velocity components along the same horizontal elevation (Figure 8b) assist in elucidation of this difference. Whereas the flow corresponding to the cases with the far ground plane show almost no vertical velocity along this horizontal axis owing to the vertical symmetry of the outer flow, the same is not true for the cases with the ground plane in the closer proximity (solid lines). The case with the lower mass flow rate engenders a downward velocity of approximately $0.3U_o$, whereas for the higher mass flow rate case, the downward velocity peaks at about U_o downstream from the inlet. These data suggest that under the short distance to the ground plane, the crosswind, interacting with the inlet suction, moves from the top of the inlet and curves down around the nacelle on the leeward side due to the offset and deflected wake. In addition, there is also an indication of negative vertical velocity within the inlet itself, which is in accord with the displaced inlet sink in the presence of a vortex (cf. Figure 7) since the sink has a negative vertical velocity component on its upper side.

For further insight into the ground vortex effect on the full flow field around the nacelle inlet, the mean streamwise velocity distributions are extracted from a sequence of the planar PIV measurements distributed along the inlet axial direction (y-direction) for the same flow condition as already shown in Figure 6d at $y = 0$. Since the role of the vectored wake flow interacting with
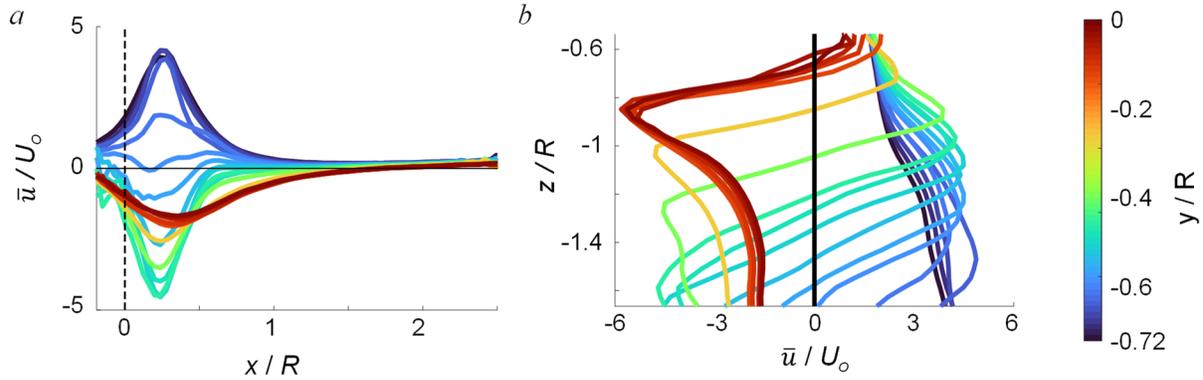
9

Figure 9. *Mean streamwise velocity through the ground vortex for $U_o = 10kt$, $\dot{m}^* = 0.3$, and $h/D = 0.36$ along a horizontal elevation at $z/R = -1.55$ (a) and along a vertical line through the vortex core at $x/R = 0.24$, for various positions along the inlet centerline $-0.72 < y/R < 0$.*

the ground plane was noted as the key precursor of the ground vortex formation, the velocity profiles are first examined in the proximity of the ground plane. Hence, Figure 9a shows the mean horizontal component of the velocity along a horizontal line located $0.15R$ from the ground plane ($z/R = -1.55$) for distances away from the inlet face ranging from $-0.72 < y/R < 0$. It is clear that these inlet-axially distributed PIV planes intersect the ground vortex that originates upstream from the inlet face at the ground plane. Starting at the point farthest from the inlet face ($y/R = -0.72$), the velocity is positive and its maximum increases towards the inlet face, reaching a maximum of $\bar{u}/U_o = 4.2$ at $y/R = -0.67$. The peak becomes nearly zero at $y/R = -0.59$ which marks the approximate location of the core of the vortex. Finally, the profiles reach a minimum of $\bar{u}/U_o = -4.4$ at $y/R = -0.51$ on the opposite side of the vortex's center. Thus, the ground vortex is nearly perfectly symmetric reaching an average maximum tangential speed of $4.3U_o$ at a distance of $0.08R$ from its core at the examined elevation of $0.15R$ above the ground plane. The position of the peaks also indicates the location of the core of the vortex at $x/R = 0.24$ on the leeward side of the inlet. Downstream from the vortex, the streamwise velocities recover to only $0.25U_o$ up to $x/R = 2.5$ – well below recovering back to freestream levels because of the impact of the vortex on the surrounding flow field.

Another look at the horizontal velocity component distributions is shown in Figure 9b along a vertical line located $0.24R$ from the center of the inlet which cuts through the core of the vortex as determined in Figure 9a. As in Figure 9a, these velocity distributions are extracted from the PIV measurements in the planes parallel to the inlet face for the inlet-axial range from $-0.72 < y/R < 0$. Interestingly, at the farthest location from the face, $y/R = -0.72$, there is a higher velocity near the ground plane than away from the surface. While the velocity in front of the inlet face is higher than the crosswind speed ($\bar{u}/U_o = 1.7$), the speed close to the ground at $y/R = -0.72$ reaches $\bar{u}/U_o = 3.9$. As the PIV plane moves closer to the inlet face (y-position increases), the velocity closest to the wall initially increases to a maximum, corresponding to the maximum discussed in Figure 9a. After this point, the velocity nearest the wall begins to decrease while increasing away from the wall. The point first experiencing negative flow in the streamwise direction is associated with crossing to the opposite side of the vortex core, which is first observed for $y/R = -0.56$, in accord with the analysis in Figure 9a. This flow eventually reaches a negative peak of $\bar{u}/U_o = -5.8$ due to the inlet suction from the windward side.

IV. Variation of the Vortex Formation Parameters

Given that the three formation parameters, namely the intake mass flow rate, crosswind speed, and ground plane distance define the flow state of the nacelle inlet flow field, the first step in elucidating possible common flow patterns under different combinations of the formation parameters is in examining how the variation of each of the parameters affects the flow field on its own. Hence, following a similar approach as before, the mean velocity along a given elevation is compared with the variation of a given condition. Considering first the effect of increasing the ground plane proximity, the streamwise velocity component is plotted along the elevation $z/R = -1.5$. For the three cases when the ground plane is the farthest away ($h/D \geq 1$),

Figure 10. *Mean streamwise velocity for $U_o = 10$kt and $\dot{m}^* = 0.3$ along a horizontal elevation at $z/R = -1.50$ for a varying ground plane distance ranging from $0.29 < h/D < 1.60$. The inlet's vertical centerline is shown black dashed for reference.*

there is no discernable difference in the velocity profiles. This is because the nacelle wake is not sufficiently vectored downward to interact with the ground plane and therefore all the air drawn into the inlet is supplied from upstream by the crosswind with no countercurrent flow close to the ground plane. For the next two closest ground plane distances, however, a velocity deficit starts to propagate from downstream which increases with the ground plane proximity. Decreasing the ground plane distance past $h/D \leq 0.44$ is observed to form a ground vortex as evidenced by the peak in the negative streamwise velocity underneath the inlet which is associated with the ground vortex flow field (cf. Figure 6d). Note that as the ground plane proximity increases, the magnitude of the negative streamwise velocity increases and migrates further towards the inlet centerline. It is noted that such a progression is in agreement with previous results [23]. It is also interesting that, while the peak velocities between the two closest ground plane distances do not vary much, the downstream velocity evolution for the closest ground plane exhibits a slower recovery towards the crosswind speed.
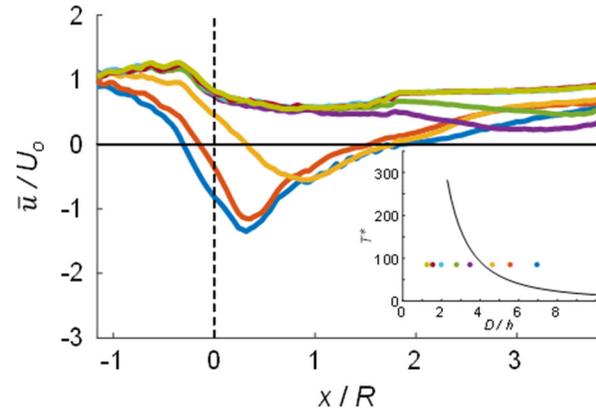
Besides the ground plane distance, the other two formation parameters – the inlet mass flow rate and crosswind speed, comprising the thrust coefficient, are varied as well. Analogous to Figure 10, Figure 11 illustrates distributions of the mean streamwise velocity component along the horizontal elevation $z/R = 1.6$. When varying the inlet mass flow rate (Figure 11a), the velocity distribution only weakly decreases from $\bar{u}/U_o \approx 1$ at the lowest flow rate and thereafter drops proportionally with the increase in the mass flow rate until the wake begins to interact with the ground plane, which is indicated by growing velocity deficit towards the ground plane, propagating from upstream. When the mass flow rate is increased such that the corresponding thrust coefficient parameter is $T^* = 53$, the magnitude of this streamwise velocity reaches zero at $x/R = 2.3$, which means that the inlet has ingested all of the upstream air close to the ground plane. Increasing the mass flow rate further up to the thrust coefficient $T^* = 67$, this streamwise velocity continues to decrease and becomes negative at the examined elevation $z/R = 1.6$, but it should be noted that no ground vortex is formed yet at this flow condition. Nonetheless, with an even further increase in the mass flow rate, the ground vortex forms and the peak in the negative velocity increases in magnitude, broadens, and shifts towards the vortex centerline, eventually reaching
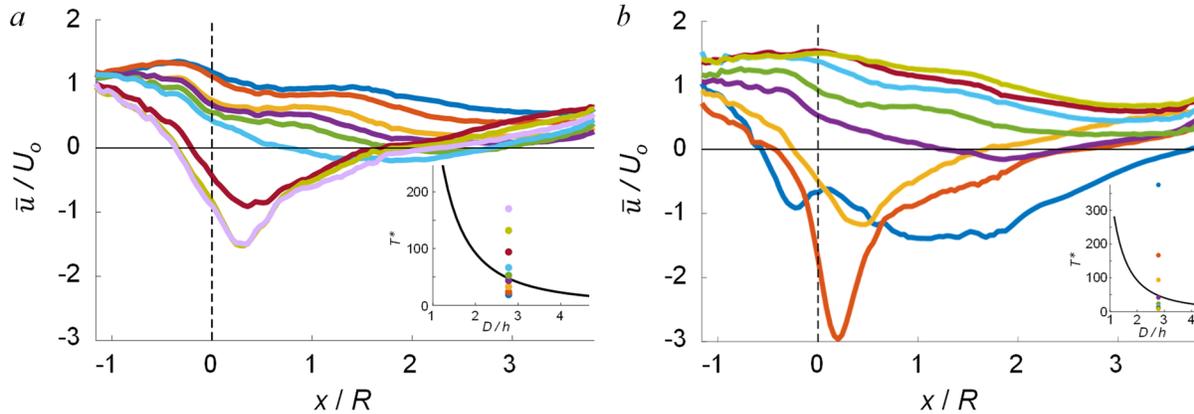
11

American Institute of Aeronautics and Astronautics

Figure 11. *Mean streamwise velocity along a horizontal elevation at z/R = -1.60 for h/D = 0.36 and varying the dimensionless thrust for U_o = 20kt by $0.26 \leq \dot{m}^* \leq 0.79$ (a) and for $\dot{m}^*$ = 0.3 by $5 \leq U_o \leq 35kt$ (b). The inlet's vertical centerline is shown black dashed for reference.*

x/R = 0.28. As already noted in Figure 10, the flow field associated with the vortex presence is also characterized with the delayed mean streamwise velocity recovery in the downstream direction.

Out of the three formation parameters, the parameter whose variation exerts the strongest effect on the inlet flow field is the crosswind speed. By definition of the thrust coefficient T^*, it is clear that small values of U_o enable large values of the thrust coefficient that are not easily attainable through variation of the other two parameters. Figure 11b shows the resulting distributions of the mean streamwise velocity component for the crosswind speed variation $5 < U_o < 35$ kt. Considering first the states that do not result in the ground vortex formation, for the highest crosswind speeds (and therefore the lowest thrust coefficient), there is no countercurrent flow towards the inlet from the ground plane, as the nacelle wake is not sufficiently vectored downward. As the crosswind speed is decreased, maintaining the same inlet mass flow rate requires more air to be drawn from the leeward nacelle side, which is indicated by the reduced streamwise velocity distributions in Figure 11b. Just as in the case of the increasing the inlet mass flow rate, with further reduction of the crosswind speed, the streamwise velocity begins to reverse direction which precedes the vortex formation. Once the crosswind speed drops below the critical level, the ground vortex does form and is identified in Figure 11b by its characteristic negative velocity peak. Decreasing the crosswind speed further from U_o = 10 to 7.5kt, the velocity magnitude near the wall triples, and its peak shifts to just downstream from the inlet centerline. Decreasing the crosswind speed even further to U_o = 5kt (T^* = 375) breaks the noted trend as, instead of a well-defined minimum, a rather broad domain of the substantial reversed flow is created with no sharp peaks, where one of the local peaks appears shifted even to the windward side of the inlet centerline. In conjunction with this effect, the downstream velocity reduction trend is much more prominent showing that, once the vortex forms, the downstream velocity can reduce significantly to the point that the velocity near the ground for U_o = 5kt is entirely negative through the full measurement domain ($x/R < 4$). The reason for this significant influx of the reversed flow is that the inlet thrust is capable of ingesting a significant portion of the wake flow on the leeward side, extending its draw down to the ground plane. This increased momentum of the flow from the leeward side can disrupt the ground vortex 'preferred' location relative to the inlet centerline and displaces the vortex to the windward side while reducing its strength, as indicated by the streamwise velocity reduction.

As seen in Figure 11b, the highest thrust coefficient velocity distribution showed a sudden departure from all other cases. When this thrust coefficient is increased even further, it is found that there is an entire sequence of 'special' cases regarding the ground vortex existence. Some of these interesting vortex realizations are illustrated in Figure 12. For $T^* = 600$ and the close ground plane proximity ($h/D = 0.36$), the ground vortex switches its typical sense of rotation and assumes the counterclockwise (CCW) sense, as shown in Figure 12a. This is presumed to result from the equally converging fronts from both the closed wake and from the windward side flow. When the ground plane is displaced further away from the inlet ($h/D = 1.6$), the critical thrust to form a vortex, despite being increased, is still achievable by further reduction in the

Figure 12. *Special vortex-state realizations for flow of exceedingly high dimensionless thrust parameter: $T^* = 600$ at $h/D = 0.36$ (a), and $T^* = 1515$ (b), 1800 (c), and 2035 (d) at $h/D = 1.60$.*

crosswind speed. At $T^* = 1515$, the closed wake becomes directly ingested along the leeward inlet side, in some instances inducing a vortex presumably formed on the outer nacelle surface, as seen in Figure 12b. Increasing the thrust coefficient further to $T^* = 1800$, the bulk inlet flow appears to swirl directly into the inlet, having the vortex core nearly centered, as shown in Figure 12c. Finally, as the crosswind speed becomes vanishingly small (and the thrust coefficient exceptionally high, $T^* = 2035$), the inlet flow appears to spawn multiple weak vortices, where the initial vortex may induce a neighboring vortex of the opposite sense, resulting in a several weak vortices distributed across the inlet, as seen in Figure 12d where three of such vortices are captured. Therefore, although the 'stable' ground vortex remains fairly well defined in terms of the nature of its formation and sense of rotation, it is also noted that there is a niche of various special vortical states that may exist in the inlet intake flow in the proximity of a ground plane, as the thrust coefficient becomes exceptionally high, eventually leading to the limit state of no vortices at the zero crosswind speed, for which the thrust coefficient would be infinite by definition.

All the discussion of the ground vortex formation up to this point suggests that the near-wall countercurrent flow presents a necessary condition for the vortex formation, and in turn, such a countercurrent flow is associated with the nacelle wake attachment to the ground plane. If the plane is at a fixed elevation relative to the inlet, this state can be attained by either increasing the intake mass flow rate or decreasing the crosswind speed (cf. Figure 11). The full measured flow field was already shown in Figure 6 and pointed to the significance of the closing wake and its associated counter flow along the surface. Furthermore, if the saddle point in the flow, which divides the flow drawn from above and below into the inlet, considered in Figures 6b and d is examined, it is clearly a good indicator of the near wake deflection. Whenever the wake is sufficiently vectored towards the ground plane and the vortex forms, the saddle point shifts down and towards the base of the inlet (Figure 6d and 13a), instead of being close to the central elevation of the inlet (e.g.,
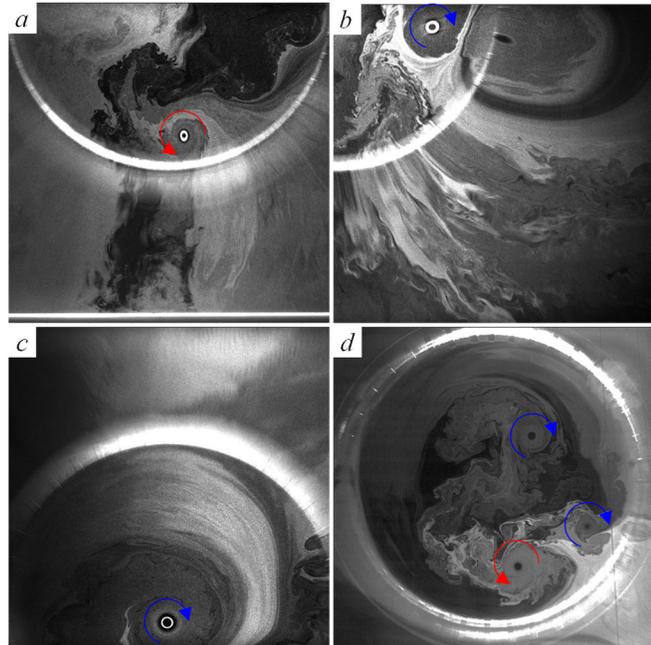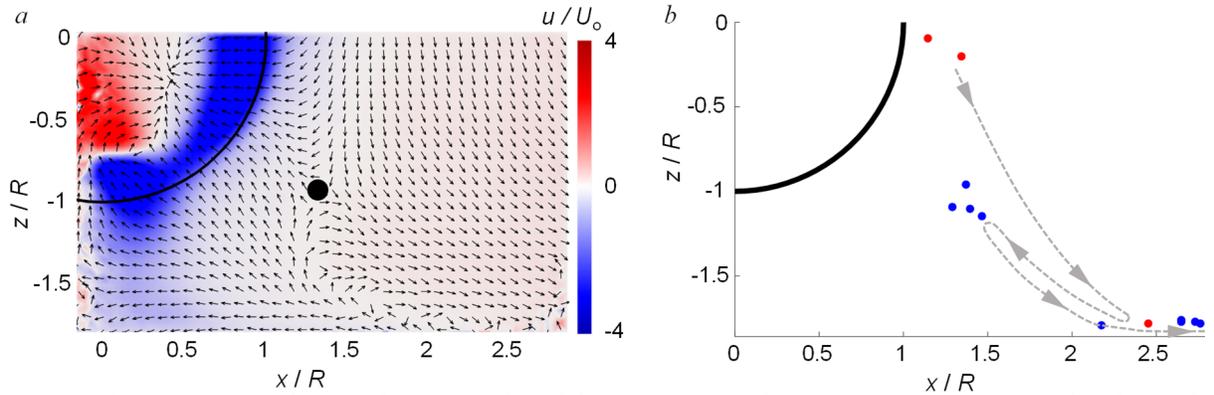
Figure 13. Time-averaged PIV color raster plot of the streamwise velocity component superposed with equal-length velocity vectors for a case with a ground vortex, marking the saddle point (a), and the migration of this saddle point with an increase of the dimensionless thrust through an increase in the inlet flow rate (b), in the presence (●) and absence (●) of a ground vortex.

Figure 6b). If this saddle point is extracted from the PIV measurements and tracked for the varying intake speed starting before the vortex forms and ending after its successive realizations, a clear pattern is observed, as illustrated in Figure 13b. At the lowest intake speeds, the saddle point, represented by red circles, is nearly coincident with the horizontal central plane of the inlet indicating that the wake is parallel to the ground plane. As the intake speed increases and the inlet begins to draw more air from the top of the inlet, the wake angles slightly downward and this results in the saddle point moving slightly downward and downstream as well. Clearly, these states do not result in the ground vortex formation. When the thrust ratio T^* reaches some critical condition for the given h/D (cf. Figure 5b), a sharp wake vectoring is effected, and the saddle point shifts to the ground plane and much further downstream ($x/R = 2.5$). This event is a precursor for the vortex formation as it initiates a negative streamwise velocity measured along the ground plane. Once the counterflow is initiated, it is a matter of increasing it to the point that the countercurrent shear layer (as discussed in Figure 4) gives a rise to the vortex within the prevailing upstream mean convection velocity, such that it can be drawn into the inlet. At that next critical condition, after the further increase in the inlet mass flow rate, the vortex is formed and ingested into the inlet. This event is marked by another sharp shift of the saddle point (marked by the blue circle in the presence of a vortex), where it migrates back upstream and upward and remains closely positioned about $x/R = 1.5$ and $z/R = -1$ at this measured position $y/R = -0.07$. If the mass flow rate is further increased beyond this 'stable' vortex state, one more and final swift change in the wake saddle point is observed as the wake will eventually fully close to the ground plane. Consequently, the saddle point shifts to the ground, moves downstream, and continues to be displaced downstream along the surface with increased inlet flow rate. It should be noted that by continuing to increase the thrust coefficient T^* through the inlet mass flow rate, the vortex state would eventually weaken and likely bifurcate to the different realizations, as discussed in Figure 12. While attaining such extremely high T^* through reduction in the crosswind speed is realizable, the operational limit on the intake mass flow rate prevents attaining these levels by that route.

As a summary of the flow states about the inlet in a crosswind with and without the influence of a ground plane, four characteristic flow fields are shown schematically in Figure 14, assuming the crosswind direction from left to right. In the absence of a ground plane, the flow is symmetrically drawn from the top and bottom of the inlet, being biased on the side of the crosswind, with the inlet sink displaced towards the leeward side (Figure 14a). If the intake mass flow rate is increased,

American Institute of Aeronautics and Astronautics

the envelope of the flow drawn into the inlet expands outward, but the flow topology does not change, preserving the top to bottom symmetry (Figure 14b). Consequently, the nacelle wake remains symmetric about the inlet axis in the mean, having the line of symmetry colinear with the inlet axis. Once the ground plane is introduced (Figure 14c), the general flow field changes somewhat even in the absence of the ground vortex formation. While most of the features discussed for the absence of the
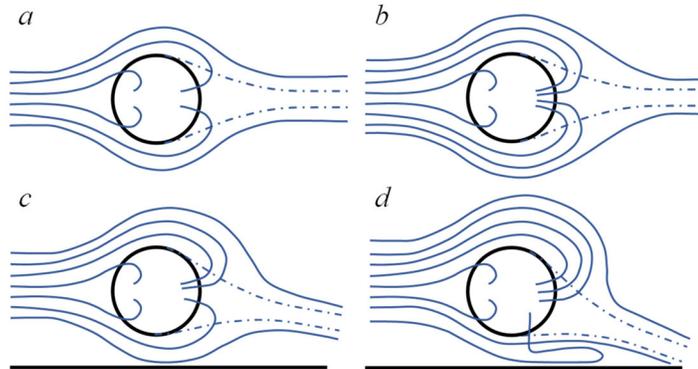

Figure 14. *Schematics of the four characteristic flow states in the absence (a-b) and presence (c-d) of a ground plane showing the effect of increasing dimensionless thrust from (a) to (b) and (c) to (d). Crosswind speed is from left to right.*

ground plane are still present, the bounding of the flow only on one side (by the ground plane) alters the flow field below the inlet relative to the unbound flow on the outer side. This alters the surrounding pressure field and consequently introduces some tilt/vectoring of the nacelle wake and breaks the horizontal flow symmetry, which was earlier shown through the measurement of a negative vertical velocity behind the inlet (Figure 8b) and by the motion of the saddle point in the wake (Figure 13b). As emphasized throughout the paper, a precursor for the vortex formation would be sufficient further vectoring of the nacelle wake such that counterflow is initiated along the ground plane. Even then, the ground vortex does not form right away (cf. Figure 13b). Only after the critical thrust coefficient T^* is reached do ground vortices begin to form within the countercurrent shear layer along the ground plane, which is created by the crosswind and the counter inlet flow after the sufficient wake-ground plane interaction (Figure 4 and Figure 14d). Not shown schematically, but it is noted that the vortex state of Figure 14d can be eventually disrupted by a further unbound increase in T^*, which would bifurcate this vortex state through a series of states that ultimately lead to the vortex dissipation and the no-vortex state as a limit state when T^* tends to infinity.

V. Scaling of the Inlet Flow Field

The vortex existence envelope expressed by Eqn. (2) does not only indicate the critical thrust coefficient T^* needed for the ground vortex formation at any ground plane distance h/D but also suggests that any flow state is uniquely defined by the two dimensionless parameters (h/D, T^*). Further, for any given ground plane distance, the flow state should be uniquely defined only by the thrust coefficient T^*. Clearly, as the same T^* can be attained through various combinations of the inlet thrust T and crosswind speed U_o, a question that can be posed is whether the vortices, or even broader – the nacelle flows, are similar for the fixed T^* but different forming parameters. To probe this similarity, instead of the full flow fields, only the velocity distributions are considered as proxies for a ground plane distance of $h/D = 0.36$, where the velocity is measured at a plane adjacent to the face of the inlet and along a line close to the ground plane at the elevation $z/R = 1.6$ (Figure 15). First, the thrust ratio $T^* = 20$ is considered that is below the critical thrust ratio required to initiate the formation of a ground vortex ($T^*_{crit} = 47$) at this h/D (cf. Figure 5b). Figure 15a indicates that all the mean streamwise velocity distributions for the varying crosswind speeds U_o = 15, 20, 25, and 30kt collapse onto the unified distribution when scaled by their respective
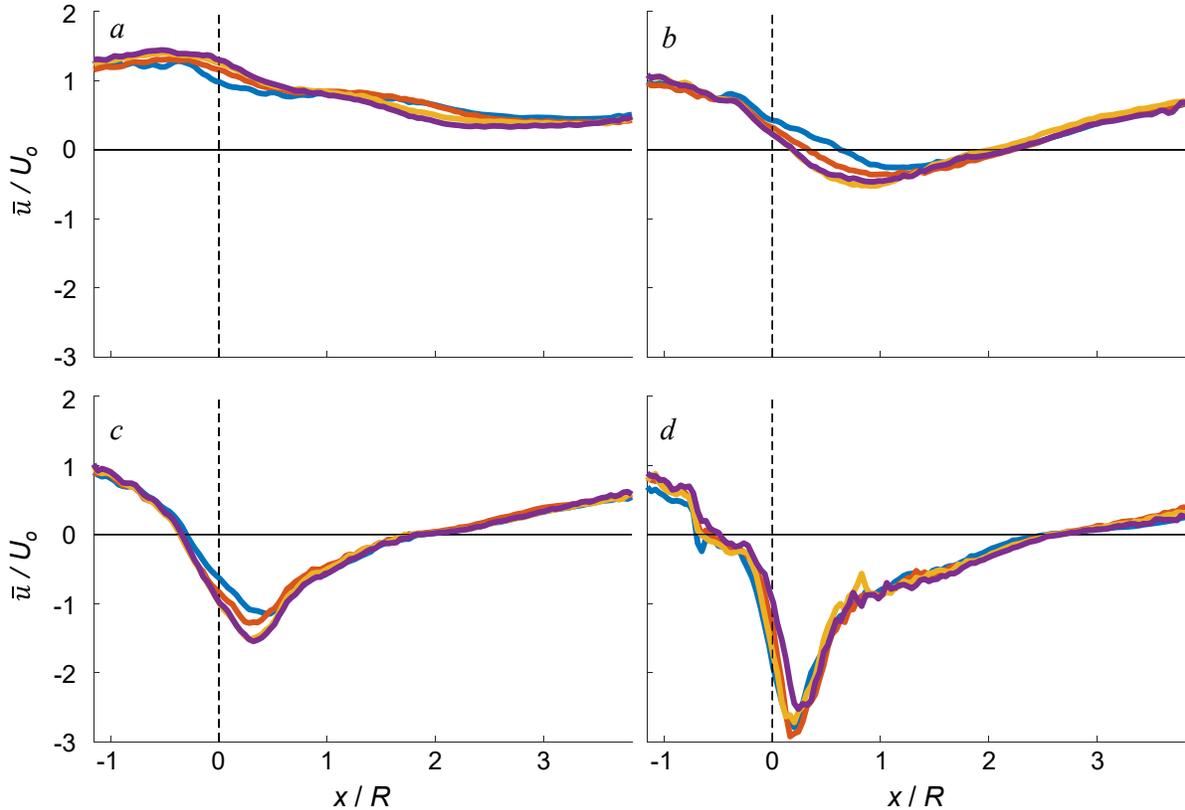
Figure 15. *Mean streamwise velocity across a plane at the inlet face along a horizontal elevation z/R = -1.60 for h/D = 0.36 and dimensionless thrust T* = 20 (a), 80 (b), 130 (c), and 250 (d).*

crosswind speed, and this distribution is characteristic for the subcritical inlet flow, prior to a ground vortex formation, already seen in Figures 10 and 11. When the thrust is increased to $T^* = 80$ (Figure 15b), this thrust ratio is above the required critical thrust to begin the onset of the vortex formation within the countercurrent shear layer; however, the thrust ratio is still not far enough beyond the critical thrust to form a stable vortex. Instantaneous PIV images show that a vortex which forms at this condition forms on the lower leeward side of the inlet and intermittently dissipates and reforms. Increasing to $T^* = 130$ (Figure 15c), the vortex is fully formed and stable, and by $T^* = 250$ (Figure 15d), the vortex gains in strength and migrates towards the inlet centerline. In addition, once the vortex forms, the downstream tunnel speed decreases as the thrust increases. Increasing the thrust ratio further ultimately induces a negative downstream velocity and a vortex on the windward side of the inlet as seen in Figure 11b for $T^* = 375$. It is remarkable that for each of the four cases in Figure 15, the scaled mean streamwise velocity near the ground plane collapses onto the unified distribution regardless of the particular values of the constitutive parameters of the nondimensional thrust T^*. For instance, for the case of $T^* = 250$ (Figure 15d), one of the flow conditions is comprised $T^*$of the inlet mass flow rate and crosswind speed of $\dot{m}^* = 0.22$ and $U_o = 5$kt, whereas another pair of parameters is about fourfold higher at $\dot{m}^* = 0.92$ and $U_o = 20$kt. Regardless of such disparate ranges, the same $T^* = 250$ for both of these flows clearly governs the flow similarity, at least within this surrogate velocity distribution analysis.

To assess whether the full inlet flow field is indeed similar, the full PIV-measured mean flow fields within a plane adjacent to the face of the inlet are compared in Figure 16. Both the flow fields in the absence ($T^* = 20$) and the presence ($T^* = 250$) of a ground vortex are considered. Two
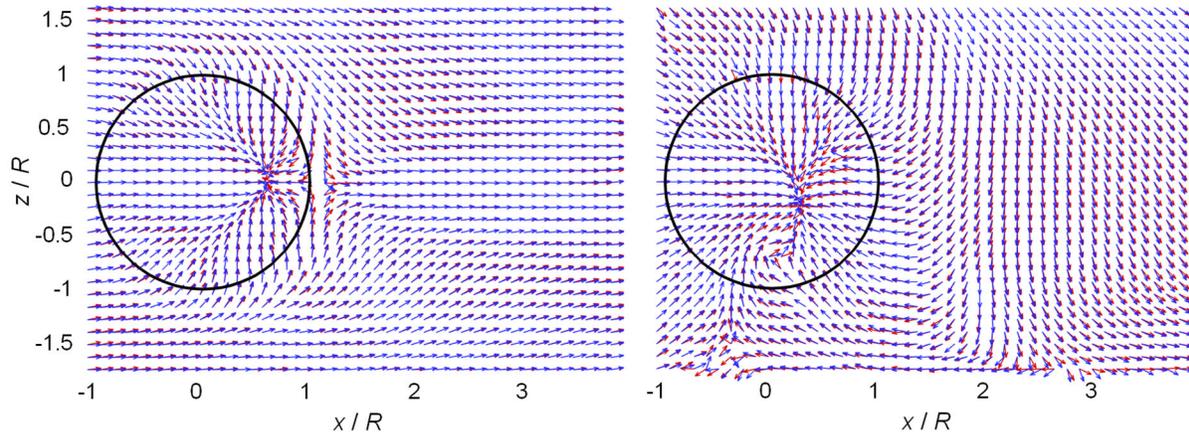
Figure 16. *Time-averaged PIV-measured velocity vectors of equal length at the inlet face plane with h/D = 0.36 and T* = 20 (a) and 250 (b) for lower (red) and higher (blue) speeds. The inlet contour is shown for reference.*

realizations of the flow field in the absence of a ground vortex are shown in two different colors in Figure 16a in terms of the mean velocity vectors, where, to emphasize the flow pattern, all the vectors are plotted of the same length, i.e., the velocity magnitude information is omitted. Both fields show strong agreement in their overall flow structure, with the largest differences arising at the location of the lowest velocity magnitudes, namely around the sink of the inlet where the motion is predominantly out-of-plane and at the saddle point in the wake where the in-plane velocity is nearly zero. Since there is no ground plane flow constraint from below, the wake is symmetric about the horizontal inlet axis. For a higher thrust ratio of $T^* = 250$ (Figure 16b), the flow structure remains remarkably similar even in the presence of a ground vortex. Just like in Figure 16a, some discrepancies are noted at the regions of the vanishing in-plane velocity, which in this flow field also include two stagnation regions where the wake closes to the ground plane and near the base of the ground vortex. Regardless of the noted zones of small discrepancies, the two flow fields are remarkably similar, particularly considering the disparate pair of the flow parameters ($\dot{m}^* = 0.22$, $U_o = 5$kt) and ($\dot{m}^* = 0.92$, $U_o = 20$kt) that comprise $T^* = 250$ of each flow field.

The previous analysis indicates that the outer flow fields for a given value of *h/D* and *T** are similar and scale with the crosswind speed, which also suggests that the internal flow through the inlet may scale as well. Given that the four different flows representing $T^* = 250$ (Figure 15d) are the most complex, color raster plots of the 72-probe total pressure rake (cf. Figure 2a) for these four flows are shown in Figure 17. At the lowest crosswind speed (Figure 17a), there are no obvious significant total pressure losses within the inlet besides those measured within the boundary layer on the windward side, although a weak imprint of the reduced pressure is also seen over the central bottom domain. Increasing the flow speeds
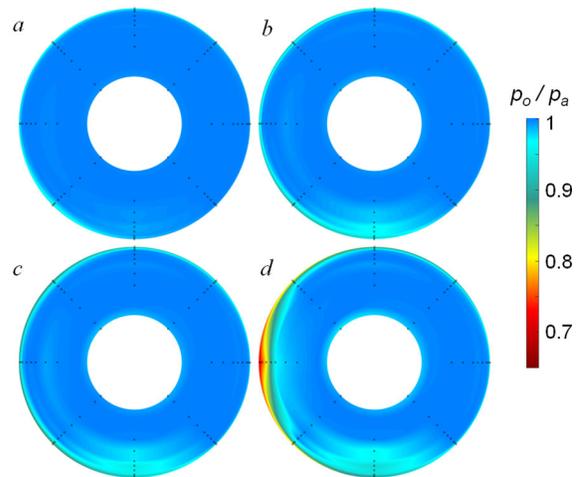

Figure 17. *Total pressure contour plots measured at the nominal location of the 'engine fan' face for h/D = 0.36 and T* = 250 attained at U_o = 10 (a), 15 (b), 17.5 (c), and 20 (d) kts.*

17

American Institute of Aeronautics and Astronautics

(Figures 17b and c), there is a stronger signature of the ground vortex measured at the total pressure rake at that central bottom inlet domain, and this signature intensifies with the crosswind speed. Interestingly, at the highest crosswind speed (Figure 17d), an even stronger total pressure deficit is measured on the inlet windward side, which is the result of flow separation as the flow is drawn around the windward inlet lip. The boundary layer cannot withstand such a sharp turn, and consequently, the flow separates as indicated by the total pressure deficit that penetrates outward away from the inner surface (e.g. [6,7]). This last example shown in Figure 17d indicates that the full internal inlet flow may not necessarily follow the scaling arguments of the outer inlet flow for a given h/D and T^*. Another possibility, not seen in Figure 17d due to the sufficient azimuthal separation, is that nominally independent events of the ground vortex ingestion and the windward flow separation can interact within the inlet, inducing a completely new flow state. This should be particularly examined for high thrust ratios as the vortex migrates toward the windward side (cf. Figure 11b) for such conditions. However, knowing that the windward flow separation typically only occurs for elevated crosswind speeds [23], this scenario is less likely as the available engine thrust may limit prevent realizations of high thrust ratios.

Despite a non-universal internal flow similarity for a given h/D and T^*, as shown in Figure 17, the ingested vortex signatures in terms of the total pressure spatial distributions in Figure 17 indicate that some local similarity about the ingested vortex might be preserved. As the vortex is nearly centered at the bottom of the inlet, this similarity is probed by plotting the radial distributions of the total pressure for the bottom rake ($\theta = 180°$, Figure 2a) for the five different flows at $h/D = 0.36$ and $T^* = 250$ (Figure 18a). As these flows were also simultaneously imaged by a PIV camera when seeded by theatrical fog, five images corresponding to each of the total pressure distributions are shown in Figure 18b. Besides an indication of the vortex flow similarity among these five flows, another interesting detail is seen in the images due to the water vapor condensation at the core of the vortex. With progressing

Figure 18. Radial distribution of total pressure deficit measured at $\theta = 180°$ for $h/D = 0.36$ and $T^* = 250$ (a) and the corresponding images of the seeded flow (b). Total pressure profiles scaled by the crosswind dynamic pressure are shown in (c). The profile in the absence of the ground vortex is shown dashed for reference.

pressure drop seen in Figure 18a, this pressure drop is manifested by the increasing domain of the vapor condensation within the vortex core. The total pressure profiles seen in Figure 18a certainly indicate similarity, even in the case with windward side flow separation (due to the decoupled flow separation from the vortex). Hence, when these radial pressure distributions associated with ingested vortices are scaled by the inertial forces of the cross flow in terms of the dynamic pressure $((p_o - p_a) / (0.5\rho U_o^2))$, all the scaled distributions collapse (Figure 18c). A total pressure distribution in the absence of a vortex is also shown for reference. The drop in the total pressure
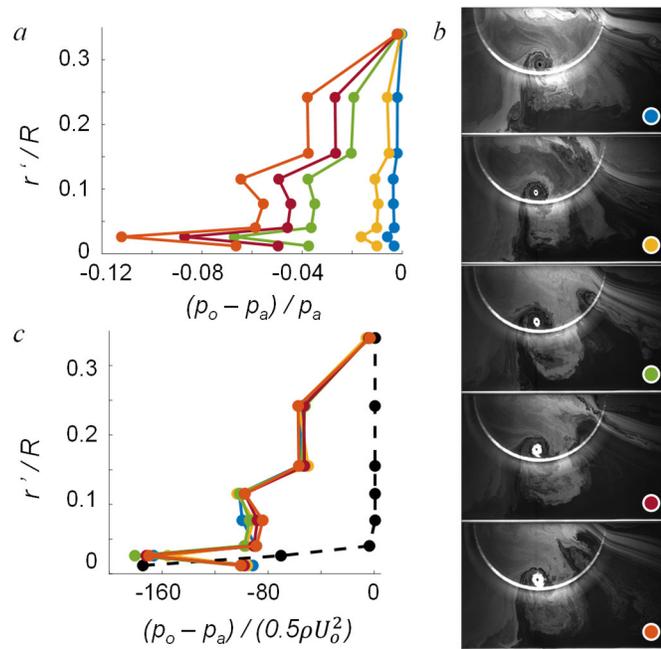
relative to such reference total pressure distribution was already utilized by Nichols et al. [23] for the ground vortex detection in the flow, where the existence of the minimum seen at $r'/R = 0.026$ is associated with the proximity of the vortex core.

VI. Conclusions

The present experimental investigations focus on the evolution of a ground vortex in the suction flow field effected by an axisymmetric nacelle inlet in the presence of a ground plane and crosswind that is normal to the nacelle's axis. It is shown that ground vortices originate within a counter-current shear layer that forms over the ground plane between the crosswind flow and the flow that is drawn into the inlet owing to the closure of the nacelle's wake onto the ground plane. Therefore, there are two critical conditions that need to be met for the ground vortex formation: i. Sufficient interaction of the nacelle's wake and the ground plane to initiate the counter flow with the crosswind towards the inlet; and ii. Sufficiently high induced velocity in this countercurrent shear layer towards the nacelle to tilt and advect spanwise vorticity concentrations off the surface boundary layer towards the nacelle's inlet. Until the second condition is met, the vortices that form within the countercurrent shear layer are advected downstream rather than form a ground vortex that is ingested by the inlet. Based on the vortex formation parameters (inlet thrust T, crosswind speed U_o, and the nacelle elevation relative to the ground plane h), it is argued that the critical thrust coefficient is related to the nacelle elevation as $T_{crit}^* = (T/(\rho U_o^2 D^2))_{crit} = 375(h/D)^2$.

The present investigations also show that, for a given flow state defined by h/D and T^*, the nacelle flow field is similar and proportional to the crosswind speed U_o. Moreover, this also holds for the internal inlet flow about the ingested vortex which is also similar as expressed by the total pressure with respect to the dynamic pressure of the crosswind. However, the similarity of the internal flow breaks within flow separation about the inlet lip along the inlet windward side. This does not affect the flow scaling about the ingested vortex as long as there is no interaction between the vortex and the separated flow.

The above discussion shows that the formation of the ground vortex can be related to the streamwise symmetry of the cross flow over the nacelle. In the absence of the ground plane, the flow above and below the nacelle in the crosswind is symmetric with respect to a horizontal center plane that intersects the nacelle's centerline. This symmetry is clearly lost in the presence of the ground plane, and the asymmetry intensifies as the elevation of the nacelle diminishes. The loss of symmetry is a precursor for the formation of a ground vortex because, in the absence of the ground plane, the streamwise evolution of the nacelle's wake is also nominally symmetric about the center plane. Once the ground plane is introduced, this symmetry is disrupted even in the absence of the ground vortex because the outer flow is bounded by the ground plane, resulting in vectoring of the nacelle's wake towards the surface. A precursor for the ground vortex formation is further vectoring of the wake by adjustment of either of the formation parameters until the wake closes on the ground plane to initiate a counter flow along the surface. Once that the critical thrust coefficient is reached, ground vortices are periodically formed within the ensuing shear layer and are ingested into the nacelle soon thereafter. It is also noted that the presence of the ground vortex is eventually disrupted by an unbound increase in T^* which ultimately leads to its dissipation and disappearance.

The present investigations indicate that the effect of the dimensionless formation parameters on the formation and evolution of the ground vortex can lead to successful development of passive and active flow control approaches to enable its suppression.

Acknowledgment

References

[1]   Trapp, L. G., Argentieri, H. G., de Souza, F. J., and Girardi, R. da M., "Aspects of Isolated Nacelles Near the Ground During Crosswind Operation," ENCIT Paper CIT06-0740, December 2006.

[2]   Colehour, J. L., and Farquhar, B. W., "Inlet Vortex," *Journal of Aircraft*, Vol. 8, No. 1, 1971, pp. 39–43. https://doi.org/10.2514/3.44224.

[3]   Trapp, L. G., and Girardi, R., "Evaluation of Engine Inlet Vortices Using CFD," AIAA Paper 2012-1200, January 2012. https://doi.org/10.2514/6.2012-1200.

[4]   Savelyev, A. A., Mikhaylov, S. V., and Zlenko, N. A., "Aerodynamic Inlet Design for Civil Aircraft Nacelle," ICAS Paper 2014-0308, September 2014.

[5]   Majić, F., Efraimsson, G., and O'Reilly, C. J., "Potential Improvement of Aerodynamic Performance by Morphing the Nacelle Inlet," *Aerospace Science and Technology*, Vol. 54, 2016, pp. 122–131. https://doi.org/10.1016/j.ast.2016.04.006.

[6]   Nichols, D. A., Vukasinovic, B., Glezer, A., DeFore, M. C., Rafferty, B., and Palacios, F. D., "Characterization and Control of Nacelle Inlet Flow in Crosswind," AIAA Paper 2019-3685, June 2019. https://doi.org/10.2514/6.2019-3685.

[7]   Nichols, D. A., Vukasinovic, B., Glezer, A., DeFore, M., and Rafferty, B., "Fluidic Control of Nacelle Inlet Flow in Crosswind," AIAA Paper 2020-2955, June 2020. https://doi.org/10.2514/6.2020-2955.

[8]   Nichols, D. A., Vukasinovic, B., Glezer, A., DeFore, M. C., and Rafferty, B., "Steady and Unsteady Control of Nacelle Inlet Flow in Crosswind," AIAA Paper 2021-1556, January 2021. https://doi.org/10.2514/6.2021-1556.

[9]   Klein, H., "Small Scale Tests on a Jet Engine Pebble Aspiration," Douglas Aircraft Co., Inc., Santa Monica Division, Publication SM 14895, 1953.

[10]   Rodert, L. A., and Garrett, F. B., "Ingestion of Foreign Objects into Turbine Engines by Vortices," NACA TN 3330, February 1955.

[11]   Siervi, F. D., "A Flow Visualization Study of the Inlet Vortex Phenomenon," Massachusetts Institute of Technology, Gas Turbine and Plasma Dynamics Laboratory, GT & PDL Report No. 159. 1981.

[12]   Johns, C., "The Aircraft Engine Inlet Vortex Problem," AIAA Paper 2002-5894, October 2002. https://doi.org/10.2514/6.2002-5894.

[13]   Liu, W., Greitzer, E. M., and Tan, C. S., "Surface Static Pressures in an Inlet Vortex Flow Field," *Journal of Engineering for Gas Turbines and Power*, Vol. 107, No. 2, 1985, pp. 387–393. https://doi.org/10.1115/1.3239738.

[14]   Shin, H. W., Greitzer, E. M., Cheng, W. K., Tan, C. S., and Shippee, C. L., "Circulation Measurements and Vortical Structure in an Inlet-Vortex Flow Field," *Journal of Fluid Mechanics*, Vol. 162, No. 8, 1986, pp. 463–487. https://doi.org/10.1017/S0022112086002124.

[15]   Nakayama, A., and Jones, J. R., "Vortex Formulation in Inlet Flow near a Wall," AIAA Paper 96-0803, January 1996. https://doi.org/10.2514/6.1996-803.

[16]   Nakayama, A., and Jones, J. R., "Correlation for Formation of Inlet Vortex," *AIAA Journal*, Vol. 37, No. 4, 1999, pp. 508–510. https://doi.org/10.2514/2.743.

[17]   Brix, S., Neuwerth, G., and Jacob, D., "The Inlet-Vortex System of Jet Engines Operating near the Ground," AIAA Paper 2000-3998, August 2000. https://doi.org/10.2514/6.2000-3998.

[18]   Siervi, F. D., Viguier, H. C., Greitzer, E. M., and Tan, C. S., "Mechanisms of Inlet-Vortex Formation," *Journal of Fluid Mechanics*, Vol. 124, 1982, pp. 173–207. https://doi.org/10.1017/S0022112082002456.

[19] Murphy, J. P., MacManus, D. G., and Sheaf, C. T., "Experimental Investigation of Intake Ground Vortices during Takeoff," *AIAA Journal*, Vol. 48, No. 3, 2010, pp. 688–701. https://doi.org/10.2514/1.45896.

[20] Murphy, J. P., and MacManus, D. G., "Ground Vortex Aerodynamics under Crosswind Conditions," *Experiments in Fluids*, Vol. 50, No. 1, 2011, pp. 109–124. https://doi.org/10.1007/s00348-010-0902-4.

[21] Shmilovich, A., and Yadlin, Y., "Flow Control Techniques for Transport Aircraft," *AIAA Journal*, Vol. 49, No. 3, 2011, pp. 489–502. https://doi.org/10.2514/1.J050400.

[22] Shmilovich, A., and Yadlin, Y., "Engine Ground Vortex Control," AIAA Paper 2006-3006, June 2006. https://doi.org/10.2514/6.2006-3006.

[23] Nichols, D. A., Vukasinovic, B., Glezer, A., and Rafferty, B, "Formation of a Nacelle Inlet Ground Vortex in Crosswind," AIAA Paper 2022-1698, January 2022. https://doi.org/10.2514/6.2022-1698.

American Institute of Aeronautics and Astronautics